Ride Dynamic Evaluations and Design Optimization of a Torsio-Elastic Off-Road Vehicle Suspension

Alireza Pazooki[1*], Dongpu Cao[2], Subhash Rakheja[1] and Paul-Émile Boileau[3]

[1]CONCAVE research Centre, Concordia University, Canada
[2]Waterloo Centre for Automotive research (WatCAR), University of Waterloo, Canada
[3]Institut de recherche Robert-Sauvé en santé et en sécurité du travail (IRSST), Montreal, Canada

e-mails: a.r.pazooki@gmail.com, dongpu@uwaterloo.ca, rakheja@alcor.concordia.ca, boileau.paul-emile@irsst.qc.ca

*Corresponding author

Abstract:
The ride dynamic characteristics of a novel torsio-elastic suspension for off-road vehicle applications are investigated through field measurements and simulations. A prototype suspension was realized and integrated within the rear axle of a forestry skidder for field evaluations. Field measurements were performed on forestry terrains at a constant forward speed of *5 km/h* under the loaded and unloaded conditions, and the ride responses were acquired in terms of accelerations along the vertical, lateral, roll, longitudinal and pitch axes. The measurements were also performed on a conventional skidder to investigate the relative ride performance potentials of the proposed suspension. The results revealed that the proposed suspension could yield significant reductions in magnitudes of transmitted vibration to the operator seat. Compared to the unsuspended vehicle, the prototype suspended vehicle resulted in nearly 35%, 43% and 57% reductions in the frequency-weighted rms accelerations along the *x*-, *y*- and *z*-axis, respectively. A 13-DOF ride dynamic model of the vehicle with rear-axle torsio-elastic suspension was subsequently derived and validated in order to study the sensitivity of the ride responses to suspension parameters. Optimal suspension parameters were identified using Pareto technique based on the genetic algorithm to obtain minimal un-weighted and frequency-weighted rms acceleration responses. The optimal solutions resulted in further reduction in the pitch acceleration in the order of 20%, while the reductions in roll and vertical accelerations ranged from 3.5 to 6%.

Keywords: Off-road vehicle ride, torsio-elastic suspension, forestry skidder ride vibration, field vibration exposure assessments, sensitivity analysis, design optimization.

1. Introduction

Wheeled off-road vehicles, employed in forestry, agriculture, mining, construction as well as military sectors are known to yield comprehensive magnitudes of low frequency ride vibration of

whole-body nature. Logging tractors used for harvesting of trees in the forestry sectors, commonly known as the skidders, are unsuspended vehicles, which yield highly complex ride vibration along the translational and rotational axes arising from dynamic interactions of the vehicle with uneven terrains. The whole-body vibration (WBV) environment of such vehicles exhibits predominance of shocks and jolts, characterized by high crest factors, particularly along the vertical and lateral axes [1,2]. It has been established that exposure to low frequency WBV encountered during skidder operation may well exceed the fatigue decreased proficiency limits defined in ISO-2631 for all the three translational axes [1]. On the basis of extensive field measurements, Cation et al. [3] showed that skidder operators' vibration exposure exceeds the health caution guidance zone for a 4-h work day, as defined in the current international standard, ISO-2631-1[2]. The measured data revealed predominance of shocks, which was characterized by a high crest factor in the vicinity of 12 in the vertical axis. Neitzel and Yost [4] further showed that the 8-h equivalent vibration exposure of forestry workers, including the skidder operators, exceeds 8-h exposure limit defined by the Commission of the European Communities [5]. The measured data further suggest that the WBV of a forestry skidder tend to dominate in the low frequency range (up to 5 *Hz*), which can be partly attributed to large diameter soft tires.

Exposure of high intensity and low frequency WBV has been widely associated with several musculoskeletal disorders among the human drivers [6-8]. Several epidemiological studies have established strong relation between exposure to WBV and low back pain (LBP) among the off-road vehicle operators [9-13]. Despite the high intensity WBV environment of forestry skidders and the associated health and safety risks, only limited efforts have been made to control the transmission of vibration to the human operator. A forestry skidder is directly suspended on large diameter soft tires, which provide only very light damping. The ride vibration properties may thus be characterized by the response of a lightly damped mechanical system. Furthermore, vehicle operations on relatively rough terrains coupled with large size tires and high location of the operator contribute to high magnitudes of lateral and fore-and-aft vibration at the operator's location. Although a number of primary and secondary suspension designs have evolved for different wheeled off-road vehicles [14-17], implementations in forestry skidders have been mostly limited to low natural frequency vertical seat suspensions [18]. This may be partly attributed to increased vehicle rollover or tip-over risk associated with a primary suspension operating on uneven forestry terrains with considerable grade and cross-grade [19,20].

Suspension seats, designed with low natural frequency in the order of 1.5 *Hz* and free travel of ± 5 *cm*, are generally employed to attenuate vertical vibration in such vehicles [21-23]. The vehicle interactions with rough forest terrains may cause the suspension seat to exceed its free travel and transmit high intensity vibration or shock motions due to end-stop impacts. Furthermore, a few studies have shown that the suspension seats used in skidders do not offer reductions in vertical vibration [3,24], while these may amplify the vibration transmitted to the operators. Alternatively, various concepts in cab suspension have evolved to attenuate vibration along the translational as well as rotational axes [25-29]. The vibration isolation performance characteristics of a prototype skidder cab supported on rubber and hydro-pneumatic mounts, and spring-damper suspension units have been investigated analytically and experimentally [26]. The study showed that the low frequency lateral vibration (predominant around 1 *Hz*) could not be attenuated by a suspension at the cab. Furthermore, the implementation of a suspension at the cab was considered to be quite complex in small size forestry vehicles, where the cab is often welded to the chassis along with the ROP structure.

Alternatively, a number of primary suspension designs have been explored for agricultural and construction vehicles to achieve improved ride comfort for operators and reduce stresses in the vehicle structure and components [14,15,30-32]. Similar developments in primary suspensions for forestry skidders have been lacking, which may be partly attributed to concerns related to reduced roll and lateral stability due to low natural frequency suspension, the requirements of high roll and pitch stiffness, complexities associated with implementation of a wheel suspension since the axles are generally welded to the chassis structure, and extreme variations in the axle loads that would pose considerable design challenge.

This study presents a concept in a torsio-elastic linkage suspension to achieve improved ride performance coupled with high lateral and roll stiffness. The performance potentials of the proposed concept are investigated analytically and through field measurements of a prototype suspension. The influences of variations in the suspension design parameters on the ride performance are further presented through a parametric study, and optimal suspension parameters are identified using the Pareto optimization based on the genetic algorithm method.

2. Ride dynamic modeling of an off-road skidder

Figure 1 schematically shows a wheeled log skidder with a single articulation. A 3 degree-of-freedom (DOF) ride dynamic model of the conventional skidder is formulated assuming constant speed operation and negligible contributions of the articulation mechanism to the vertical, roll and pitch responses. Considering that the axles are welded to the vehicle frame, the frame together with the axles and the cabin can be considered as a rigid mass supported on four tires, which are modeled by linear damped springs with point contact with the terrain, as illustrated in the pitch and roll-plane models in Fig. 2. The equations of motion for the vehicle model subject to terrain excitations at the four tire-terrain contact points are derived as follows:

$$m_s\ddot{z}_s + \sum_{1}^{4} F_{Ti} = 0;\ I_{YYS}\ddot{\theta}_s - WB_1\left[F_{T1}+F_{T2}\right] + WB_2\left[F_{T3}+F_{T4}\right] = 0 \qquad (1)$$

$$I_{XXS}\ddot{\phi}_s + T\left[F_{T1}+F_{T3}\right] - T\left[F_{T2}+F_{T4}\right] = 0$$

where m_s, I_{YYS} and I_{XXS} are the mass, and pitch and roll mass moments of inertia of the vehicle, respectively. T is the half track width, assumed to be identical for both axles, and WB_1 and WB_2 are longitudinal coordinates of the front and rear axles with respect to vehicle center of gravity (cg). z_s, θ_s and ϕ_s are vertical, pitch and roll displacements, respectively, of the sprung mass about a static equilibrium, and $F_{Ti} = K_{Ti}q_i + C_{Ti}\dot{q}_i$ is the force developed by tire i (i=1,2,3,4), where K_{Ti} and C_{Ti} are the linear stiffness and damping coefficients of tire i, and q_i is its deflection, given by:

$$q_i = z_s + (-1)^j WB_j\theta_s + (-1)^i T\phi_s - z_{0i}; \qquad j=1 \text{ for } i=1,2;\ \text{and } j=2 \text{ for } i=3,4. \qquad (2)$$

where z_{0i} is the terrain elevation at the interface of tire i.

2.1 Torsio-elastic suspension concept

The torsio-elastic suspension consists of a linkage that is oriented along the vehicle lateral axis and couples the vehicle body (sprung mass) with the unsprung mass. The suspension linkage mechanism envelopes two 0.6 *m* long tubular shafts of elliptical cross section (43 *mm* × 38 *mm*), oriented along the vehicle longitudinal axis, directly coupling the sprung and unsprung masses through a series of clevises, as illustrated in Fig. 3(a). Each tubular shaft comprises an elastomeric bar reinforced with a 16 *mm* metallic shaft in the center. The nominal width of the suspension link is 160 *mm*, while its length could be varied depending upon the desired load carrying capacity. The torsio-elastic suspension is introduced at the rear axle of the vehicle by eliminating the rigid coupling between the chassis and the rear axle, while providing high effective roll stiffness due to restoring moment capability of the torsional shafts. A pictorial view of the suspension fitted to the rear axle of a skidder is shown in Fig. 3(b), while the suspension with the sprung and unsprung masses in the roll plane is schematically shown in Fig. 3(c). The laterally-oriented linkage suspension undergoes relative roll motions between the unsprung and sprung masses, which yields a kinematic advantage and absorption of energy due to torsional deflections of each composite shaft. In addition, the composite shaft could also undergo radial deflection.

2.2 Development of a ride dynamic vehicle model with rear-axle suspension

The log skidder, retrofitted with the proposed torsio-elastic suspension at the rear-axle, is analytically modeled as a 13-DOF dynamic system. Figures 4(a) and 4(b) illustrate the pitch and roll planes of the full-vehicle model with the rear-axle suspension, respectively, while the detailed linkage suspension model is shown in Fig. 4(c). The vehicle body, chassis, cab, and the mounted equipment together with the front axle are represented by a lumped sprung mass (m_s') with four-DOF: vertical (z_s), roll (ϕ_s), pitch (θ_s), and lateral (y_s). The rear axle is represented by a rigid body with three-DOF: vertical (z_{ur}), lateral (y_{ur}), and roll (ϕ_{ur}). Each suspension link on the right and left sides is considered to possess three-DOF motion along the vertical (z_3, z_4), roll (ϕ_3, ϕ_4), and lateral (y_3, y_4) directions. Each tire is modeled as a parallel combination of linear energy restoring and dissipative elements, assuming that the tire remains in contact with the terrain through a point contact model. The torsio-elastic suspension is characterized by its radial and torsional visco-elastic properties. The radial visco-elastic properties are represented by linear stiffness and damping elements along the vertical (k_z, c_z) and lateral (k_y, c_y) axes, while the torsional properties are characterized by linear torsional stiffness and damping coefficients (k_t, c_t).

The equations of motion for the vehicle model subject to terrain excitations at the four tire-terrain contacts points are formulated as follows:

$$m_s'\ddot{z}_s + \sum_{i=1}^{2} F_{Ti} + \sum_{i=3}^{4}\left(F_{zi}\right) = 0\,; \qquad m_s'\ddot{y}_s + \sum_{i=3}^{4} F_{yi} + \sum_{i=1}^{2} F_{TYi} = 0$$

$$I_{XXS}'\ddot{\phi}_s + M_{\theta 4s} + M_{\theta 3s} - \left(F_{z4} - F_{z3}\right)L_1 - \sum_{i=3}^{4} F_{yi}h - T\left(F_{T2} - F_{T1}\right) + \sum_{i=1}^{2} F_{TYi}\left(h + h_1 + R\right) = 0$$

$$I_{YYS}'\ddot{\theta}_s + \sum_{i=3}^{4} F_{zi}WB_2 - \sum_{i=1}^{2} F_{Ti}WB_1 = 0$$

$$m_{ur}\ddot{z}_{ur} + \sum_{i=3}^{4} F_{Ti} - \sum_{i=3}^{4} F_{ziu} = 0\,; \qquad m_{ur}\ddot{y}_{ur} - \sum_{3}^{4} F_{yiu} + \sum_{i=3}^{4} F_{TYi} = 0$$

$$
\begin{aligned}
&I_r\ddot{\phi}_{ur}+(F_{T3}-F_{T4})T-\sum_{i=3}^{4}\left[RF_{TYi}+F_{yiu}h_1-F_{ziu}(L_1+L_0)\right]-M_{\theta 3u}-M_{\theta 4u}=0\\
&m_3\ddot{z}_3+F_{z3u}-F_{z3}=0; \qquad\qquad m_4\ddot{z}_4+F_{z4u}-F_{z4}=0\\
&I_3\ddot{\theta}_3+(F_{z3u}+F_{z3})\frac{L_0}{2}-M_{\theta 3s}+M_{\theta 3u}=0; \qquad I_4\ddot{\theta}_4+(F_{z4u}+F_{z4})\frac{L_0}{2}-M_{\theta 4s}+M_{\theta 4u}=0\\
&m_3\ddot{y}_3+F_{y3u}-F_{y3}=0; \qquad\qquad m_4\ddot{y}_4+F_{y4u}-F_{y4}=0
\end{aligned}
\tag{3}
$$

where I'_{XXS} and I'_{YYS} are roll and pitch mass moments of inertia of the sprung mass, respectively. I_r, I_3 and I_4 are the roll mass moments of inertia due to rear axle, and right and left suspension links, respectively. The geometric parameters L_0, L_1, R, h and h_1 are illustrated in Fig. 4. In the above equations, subscripts "3" and "4" of the forces or moments refer to those developed by the right- and left-suspension units, respectively. F_{z4} and F_{z3} are vertical forces acting on the sprung mass developed due to left- and right-axle suspensions, respectively. F_{z3u} and F_{z4u} are the corresponding forces acting at the unsprung mass attachments. (F_{y3}, F_{y4}) and (F_{y3u}, F_{y4u}) are the lateral forces acting on the sprung and unsprung masses, respectively, due to radial stiffness and damping properties of the torsio-elastic suspension, and ($M_{\theta 3s}$, $M_{\theta 4s}$) and ($M_{\theta 3u}$, $M_{\theta 3u}$) are the respective roll moments acting on the sprung and unsprung masses. F_{TYi} $(i=1,...,4)$ are lateral forces developed at the tire-terrain interfaces. The forces and moments developed due to the tire and suspensions are described in details in the Appendix.

The coupled differential equations of motion of the 13-DOF skidder model can be expressed in the following matrix form:

$$
[M]\{\ddot{q}\}+[C]\{\dot{q}\}+[K]\{q\}=[C_F]\{\dot{q}_0\}+[K_F]\{q_0\} \tag{4}
$$

where [M], [C] and [K] are (13×13) mass, damping and stiffness matrices, respectively, and $[C_F]$ and $[K_F]$ are (13×4) forced damping and stiffness matrices. $\{q\}$ and $\{q_0\}$ are the vectors of generalized and excitation coordinates, given by:

$$
\begin{aligned}
\{q\}&=\{z_s, \phi_s, y_s, \theta_s, z_{ur}, \phi_{ur}, y_{ur}, z_3, \theta_3, y_3, z_4, \theta_4, y_4\}'\\
\{q_0\}&=\{z_{01}, z_{02}, z_{03}, z_{04}\}'
\end{aligned}
\tag{5}
$$

The superscript " ' " in the above equations denotes the transpose. The equations of motion of the 3-DOF unsuspended vehicle can also be presented in the matrix form of Eq. (4), where the generalized coordinate vector is $\{q\}=\{z_s, \theta_s, \phi_s\}'$.

3. Field measurements of vehicle ride vibration responses

Field tests were performed to measure and compare the ride vibration characteristics of a conventional unsuspended skidder and a skidder fitted with the proposed torsio-elastic suspension at the rear axle. The two vehicles (TREE FARMER C6D) were identical in all respects except for the rear-axle suspension. Both the vehicles employed a cushioned seat

without a suspension and were instrumented to measure the vibration responses at the cabin floor along the vertical, fore-aft, lateral, roll and pitch directions during the transport operation under loaded and unloaded conditions. The measured data were analyzed to obtain relative ride properties of the suspended and unsuspended vehicles. The data acquired with the unsuspended vehicle were further applied to obtain an estimate of the terrain properties, while those with the suspended vehicle were used to examine validity of the 13-DOF ride dynamic model and to assess the potential ride benefits of the proposed suspension.

3.1 Measurement methods and data analyses

A total of six accelerometers were installed on the cabin floor of each vehicle to measure vibration responses along the fore-aft (x), lateral (y), vertical (z), roll (ϕ) and pitch (θ) axes. Figure 5 illustrates a schematic of the accelerometers located at the cab floor, together with the distances between the various accelerometers. One accelerometer was mounted beneath the driver seat to capture vertical vibration near the driver seat, indicated as "4". Three accelerometers, "1", "2" and "3", oriented along x, y and z-axes, respectively, were installed at rear-left of the cabin, and two single-axis accelerometers were mounted at the front-left, "5", and front-right, "6", of the cabin at the floor level. The roll and pitch acceleration response characteristics of each vehicle were derived from the measured vertical accelerations using kinematic relations, while assuming small angular motions and negligible contribution due to structure flexibility, such that:

$$\ddot{\phi}_c = \frac{\ddot{z}_5 - \ddot{z}_6}{B}; \ \ and \quad \ddot{\theta}_c = \frac{\ddot{z}_3 - \ddot{z}_5}{L} \tag{6}$$

where $\ddot{\phi}_c$ and $\ddot{\theta}_c$ are roll and pitch accelerations of the vehicle cabin, respectively, and $\ddot{z}_5$, $\ddot{z}_6$ and $\ddot{z}_3$ are vertical accelerations measured at locations 5, 6 and 3, respectively, as shown in Fig. 5. The lateral spacing between accelerometers 5 and 6 is denoted by B, and L is longitudinal spacing between accelerometers 3 and 5.

It should be noted that measurements of vibration levels at the operator seat were not attempted, since such vehicles may employ widely different types of seats with or without a suspension. The vibration transmitted to the driver's seat, however, was evaluated for exposure assessment. For this purpose, the fore-aft ($\ddot{x}_{m0}$) and lateral ($\ddot{y}_{m0}$) acceleration levels at the driver-seat interface were estimated from those measured at the cab floor, assuming small rotations and negligible effects of the seat cushion, such that:

$$\ddot{x}_{m0} = \ddot{x}_1 - h\ddot{\theta}_c; \quad and \quad \ddot{y}_{m0} = \ddot{y}_2 + h\ddot{\phi}_c \tag{7}$$

where h is the seat height from the cabin floor, and $\ddot{x}_1$ and $\ddot{y}_2$ are the longitudinal and lateral accelerations measured at the cab floor using accelerometers 1 and 2, respectively (Fig. 5). Although the seat cushion was expected to influence the cab floor vibration transmitted to the operator, particularly at frequencies above 3 Hz, the vertical acceleration ($\ddot{z}_4$), measured beneath the seat, was considered for the exposure assessment, such that $\ddot{z}_{m0} = \ddot{z}_4$, where $\ddot{z}_{m0}$ is the vertical acceleration at the operator-seat interface.

The measurements were performed while the two vehicles were driven in a forest in Eastern Quebec (Canada) by the same driver. The driver was advised to operate the vehicle at a steady speed near 5 *km/h*, and the accelerometers signals were acquired in a multi-channel data recorder. The measurements were acquired while the vehicles were driven forward along the selected trails and return to the start location. The duration of each measurement ranged from 5 to 15 minutes. The measured signals were manipulated to compute the roll and pitch accelerations of the cabin using Eq. (6), and the acceleration responses at the seat ($\ddot{x}_{m0}, \ddot{y}_{m0}, \ddot{z}_{m0}$) using Eq. (7). The time histories of the resulting acceleration signals were subsequently analyzed using a multi-channel signal analyzer to derive power spectral density (PSD) spectra of accelerations along the fore-aft, lateral and vertical-axes at the seat, and along the fore-aft, lateral, vertical, roll and pitch axes at the cab floor.

The spectra were evaluated using a bandwidth of 100 *Hz* and frequency resolution of 0.125 *Hz* considering a 75% overlap. The overall unweighted and frequency-weighted rms accelerations at the seat were also obtained for relative ride assessments of the suspended and unsuspended vehicles. The frequency-weighted rms accelerations were computed using the W_k–, W_d– and W_e–weighting filters defined in ISO-2631-1 [2] for vertical, horizontal and angular accelerations, respectively.

4. Response analyses of the vehicle model

The coupled differential equations of motion for the 3-DOF and 13-DOF models of the conventional and suspended vehicle models, respectively, were solved in the frequency-domain to obtain ride vibration responses at the operator seat and cab floor. The spectral densities of the generalized response coordinates could be derived from the complex frequency response function of the models, such that:

$$[S(j\omega)] = [H(j\omega)][S_i(j\omega)][H(j\omega)]^{'*} \tag{8}$$

where $[H(j\omega)]$ is the (3×4) and (13×4) complex transfer function matrices of the conventional and suspended vehicle models, respectively. The superscript "$'^*$" denotes the transposed complex conjugate of the transfer function matrix. In the above equation, $[S(j\omega)]$ is the spectral density matrix of the generalized response coordinates, and $[S_i(j\omega)]$ is the (4×4) matrix of the spectral density of elevations at the four tire-terrain interfaces, given by:

$$[S_i(j\omega)] = \sigma \begin{bmatrix} 1 & e^{-i\omega\tau_\phi} & e^{-i\omega\tau_\theta} & e^{-i\omega(\tau_\phi+\tau_\theta)} \\ e^{i\omega\tau_\phi} & 1 & e^{-i\omega(\tau_\phi-\tau_\theta)} & e^{-i\omega\tau_\theta} \\ e^{i\omega\tau_\theta} & e^{i\omega(\tau_\phi-\tau_\theta)} & 1 & e^{-i\omega\tau_\phi} \\ e^{i\omega(\tau_\phi+\tau_\theta)} & e^{i\omega\tau_\theta} & e^{-i\omega\tau_\phi} & 1 \end{bmatrix} \tag{9}$$

where σ is the amplitude of the terrain elevation, which is related to the vehicle speed V and the spatial PSD of the terrain roughness $G_Z(\Omega)$ as a function of the spatial frequency Ω of the terrain profile, such that: $\sigma(\omega) = G_Z(\Omega)/V$. τ_θ defines the correlation between the front and rear wheels in the pitch plane, and τ_ϕ describes the correlation between the right- and left- wheels in

the roll plane. The correlation between the front and rear wheels excitation can be expressed as a function of the vehicle speed and the wheelbase [33], such that $\tau_\theta = WB/V$.

The roll excitation due to unevenness of the two tracks of the terrain is estimated by generating a randomly distributed cross-slope function in the following manner:

$$\chi = 2T(0.5 - rnd) \tag{10}$$

where rnd is a Gaussian random number generated between 0 and 1. The random cross-slope is expressed in terms of an equivalent time delay between the right- and left-wheels in a manner similar to that described for the front- and rear-axle wheels, such that $\tau_\phi = \chi/V$.

The response characteristics at the driver-seat location ($\ddot{x}_{s0}, \ddot{y}_{s0}$, $\ddot{z}_{s0}$) are evaluated using the coordinate transformations. The frequency response transfer function matrix relating displacement responses at the seat (x_{s0}, y_{s0}, z_{s0}, θ_{s0}, ϕ_{s0}) to the generalized coordinates is formulated as:

$$[H_{s0}(j\omega)] = [R][H(j\omega)] \tag{11}$$

where [R] is (5×3) or (5×13) coordinate transformation matrix relating the generalized coordinates with those at the operator seat for the conventional and suspended vehicle models, respectively. $[H_{s0}(j\omega)]$ is the (5×4) frequency response function matrix relating the response vector at the seat to the excitation coordinates. The PSD of displacement responses at the seat can be subsequently evaluated from:

$$[S^d_{s0}(j\omega)] = [H_{s0}(j\omega)][S_i(j\omega)][H_{s0}(j\omega)]^{*} \tag{12}$$

where $[S^d_{s0}(j\omega)]$ is the (5×5) matrix of PSD of displacement responses at the seat. The PSD of acceleration response at the seat $[S^a_{s0}(j\omega)]$is subsequently computed from:

$$[S^a_{s0}(j\omega)] = \omega^4[S^d_{s0}(j\omega)] \tag{13}$$

4.1 Estimation of an equivalent terrain profile

The analysis of ride dynamic model of the forestry skidder requires characterization of roughness properties of the forestry terrain. Although the surface roughness properties of various undeformable off-road terrains have been characterized and expressed by regression models in many studies [34-36], a description of a forestry terrain could not be found. Furthermore, the surface roughness of a forestry terrain may vary with local soil properties and number of passes of the vehicle [37,38]. In this study, roughness of the forestry terrain is estimated from the measured responses of the unsuspended vehicle in conjunction with its 3-DOF model. For this purpose, the 3-DOF vehicle model was initially analyzed by considering a random terrain excitation derived from a roughness model of the form [39]:

$$G_Z(\Omega) = \alpha \Omega^{-\beta}; \quad \alpha > 0 \; and \; \beta > 0 \tag{14}$$

where constants α and β are the roughness coefficient and waviness of the terrain, respectively, which are generally identified from measured roughness profiles. The temporal frequency of the terrain excitation is computed from $f=\Omega V$. The constants α and β were identified from the measured responses of the conventional skidder. For this purpose, a minimization problem was formulated to minimize sum of squared normalized errors between the model and the measured responses at the vehicle *cg* at several discrete frequencies, such that:

$$\varepsilon(\omega, \alpha, \beta) = \sqrt{\left(\frac{\mathrm{Re}\left(S^a(1,1)\right) - \ddot{z}_c}{\ddot{z}_c}\right)^2 + \left(\frac{\mathrm{Re}\left(S^a(2,2)\right) - \ddot{\theta}_c}{\ddot{\theta}_c}\right)^2 + \left(\frac{\mathrm{Re}\left(S^a(3,3)\right) - \ddot{\phi}_c}{\ddot{\phi}_c}\right)^2} \tag{15}$$

where ε is the error function corresponding to a discrete circular frequency ω. $S^a(i,i), i = 1,2,3$ are the vertical, pitch and roll acceleration responses of the unsuspended vehicle model, respectively.

In the error function, $\ddot{z}_c$ refers to the measured vertical acceleration transformed to the vehicle *cg*, which is estimated from the measured vertical acceleration beneath the seat ($\ddot{z}_4$), and measured roll ($\ddot{\phi}_c$) and pitch ($\ddot{\theta}_c$) accelerations of the cabin:

$$\ddot{z}_c = \ddot{z}_4 + l_x \ddot{\theta}_c + l_y \ddot{\phi}_c \tag{16}$$

where l_x and l_y are longitudinal and lateral distances between the vehicle *cg* and the seat base, respectively, as shown in Fig. 2.

The minimization problem was solved at 150 different discrete frequencies of excitation in the 0.375 to 25 *Hz* range using Matlab optimization toolbox [40], assuming a constant forward speed of 5 *km/h*. The starting values of parameters were taken as those for a plowed field $\left(\alpha = 6.5 \times 10^{-4} \; ; \; \beta = 1.6\right)$ [39]. The solutions were also attempted for different starting values, which converged to very similar values of the parameter vector at each frequency. The solutions of the minimization problem provided the parameter vector values corresponding to each discrete frequency, which showed considerable variation with the frequency. The identified coefficients were subsequently applied to the roughness model in Eq. (14) to determine terrain roughness in terms of spatial PSD of the profile, $G_Z(\Omega)$. Figure 6 illustrates variations in spatial PSD as a function of the spatial frequency Ω. The results clearly show considerable scatter in the spatial PSD data. A power regression function of the form, defined in Eq. (14), was subsequently fitted to the data to obtain estimates of the probable roughness coefficients, which resulted in the following roughness model with a correlation coefficient (r^2) value of 0.6425.

$$G_Z(\Omega) = 1 \times 10^{-4} \Omega^{-1.7528} \tag{17}$$

The above roughness model of the forestry terrain may be considered to represent roughness profile of an equivalent undeformable terrain. The identified roughness model coefficient and the

roughness profile are compared with those reported for the plowed field and pasture [39], and the MVEE (Military Vehicle Engineering & Establishment) random course [34,36], in Table 1 and Fig. 7, respectively. The comparisons suggest lower roughness of the forestry terrain compared to the profiles considered, particularly corresponding to the lower wave numbers. This may also be attributed to relatively soft forestry terrain since the measurements were performed during late fall season. The waviness of the forestry terrain, however, is quite comparable to those of the plowed field and the pasture.

Table 1: Comparisons of roughness model coefficients (α, β) with those reported for some of the off-road terrains [34,36,39].

Terrain	α	β
Plowed	6.50×10^{-4}	1.60
Pasture	3.00×10^{-4}	1.60
MVEE	3.16×10^{-4}	2.27
Present Study	1.00×10^{-4}	1.76

5. Results and discussions

The measured vibration responses of both the suspended and unsuspended vehicles were compared to assess effectiveness of the proposed torsio-elastic suspension in reducing transmission of terrain-induced vibration to the cabin and the human driver's location. The responses were evaluated in terms of power spectral densities of accelerations, overall rms accelerations along all the axes, as well as 8-hour energy frequency-weighted acceleration [2,5]. Figure 8 compares PSD of accelerations measured at the cabin floor of both the suspended and unsuspended loaded vehicles along the fore-aft, lateral, vertical, pitch and roll axes. The results suggest that the predominant fore-aft and lateral vibration occur at frequencies near or slightly below 1 *Hz*, which are attributable to the pitch and roll modes resonances, respectively. For both the vehicles, the roll, pitch, and vertical acceleration peaks occur near the respective resonance frequencies of 1.0 *Hz*, 0.9 *Hz* and 1.6-2.1 *Hz* range, respectively. Although the resonance frequencies of both the vehicles appear to be quite comparable, the suspended vehicle yields significantly lower magnitudes of vibration in all the axes when compared to those of the unsuspended vehicle.

The potential benefits of the proposed torsio-elastic suspension were also evaluated from the overall unweighted and weighted acceleration responses, computed in the 0.5-20 *Hz* frequency range, and the 8-hour energy frequency-weighted acceleration. The frequency-weighted rms accelerations along the *x*-, *y*- and *z*-axis at the driver's location were evaluated through applications of the appropriate weighting functions defined in ISO-2631-1 [2]. The total WBV exposure was also evaluated in terms of vector summation of the weighted accelerations along the three translational axes, such that:

$$a_v = \sqrt{\left(k_x^2 a_{wx}^2 + k_y^2 a_{wy}^2 + a_{wz}^2\right)} \tag{18}$$

where a_{wx} and a_{wy} are W_d-weighted rms fore-aft and lateral accelerations, respectively, and a_{wz} is the W_k-weighted rms vertical acceleration. The constants k_x and k_y are additional weightings used to account for human sensitivity to horizontal vibration, as recommended in ISO-2631-1 [2].

Eight-hour energy equivalent frequency-weighted acceleration *A(8)* is also computed in accordance with the exposure assessment guidelines of EC [5], which is computed from:

$$A(8) = a_v \sqrt{\frac{T_e}{T_0}} \tag{19}$$

where T_0 is the reference duration of 8 hours and T_e is the average daily exposure duration. In this study, the average daily exposure duration is taken as 4 hours on the basis of the information attained from the Forestry Engineering Research Institute of Canada [41].

Table 2 summarizes the unweighted and frequency-weighted rms accelerations along each axis of the suspended and unsuspended vehicles with and without the load. The Table also presents the total exposure a_v and *A(8)* values. The results show that the torsio-elastic suspension could significantly decrease the vibration exposure levels in all the directions. The suspended vehicle yields 35%, 43% and 57% lower frequency-weighted rms accelerations in *x*-, *y*- and *z*-axis, respectively, compared to the unsuspended vehicle, when loaded. The suspended vehicle, however, exhibits relatively higher unweighted pitch and roll vibration, when unloaded, while the unweighted rms accelerations along the *x*, *y*, and *z* directions are 44%, 27% and 45% lower, respectively, compared to those of the unsuspended vehicle. The higher pitch response of the suspended vehicle is attributed to the pitch dynamic response of the vehicle with a relatively soft suspension at its rear axle. This phenomenon has been illustrated by Cao et al. [42]. The results further show that the weighted magnitudes of horizontal vibration transmitted to the operator location are either comparable to or exceed vertical vibration magnitude. The results also suggest that both the a_v and *A(8)* values for the suspended vehicle are 41% and 37% lower than those of the unsuspended vehicle under the loaded and no-loaded conditions, respectively. The results thus suggest that the proposed torsio-elastic suspension could offer considerable benefits in reducing the WBV exposure of the vehicle operators.

Table 2: Comparisons of unweighted and frequency-weighted rms accelerations along individual axes, the overall rms acceleration and 8-hour energy equivalent values of the suspended and unsuspended vehicles with/without load at the driver location.

Axis	Unweighted rms acceleration, m/s^2				Frequency-weighted rms acceleration, m/s^2			
	Loaded		Unloaded		Loaded		Unloaded	
	Unsusp.	Susp.	Unsusp.	Susp.	Unsusp.	Susp.	Unsusp.	Susp.
x	1.39	0.85	1.59	0.89	1.16	0.75	1.43	0.78
y	2.12	1.26	1.79	1.30	1.67	0.95	1.52	1.07
z	2.34	1.00	1.83	1.00	1.41	0.60	1.12	0.62
θ	1.01	0.74	0.70	0.82	0.72	0.52	0.46	0.43
ϕ	2.01	0.79	1.10	2.00	1.53	0.56	0.75	0.44
a_v					3.03	1.80	3.13	1.96
A(8)					2.14	1.27	2.21	1.40

5.1 Vehicle model validation

Validity of the 13-DOF ride dynamic model was examined using the field-measured data corresponding to the unloaded case, which could serve as a design tool for deriving an optimal suspension design. The ride dynamic responses of the vehicle model were obtained under terrain

excitation defined in Eqs. (9) and (17), assuming a constant vehicle speed of 5 *km/h*, which is identical to that used for the field measurements. The simulation parameters of the vehicle model are summarized in Table 3, which were obtained partly from the data sheets provided by the manufacturers, and partly estimated from the measured natural frequencies of the vehicle [46].

The results obtained from the eigenvalue problem for the vehicle model revealed vertical, pitch and roll mode resonance frequencies of the sprung mass near 2 *Hz*, 1.1 *Hz* and 0.9 *Hz*, which are quite close to the frequencies corresponding to the peaks in the measured acceleration spectra (Fig. 8), while the resonant frequencies of the unsprung mass and the suspension linkage mechanisms were significantly higher. The ride vibration responses of the vehicle model near the operator seat were subsequently obtained in terms of acceleration PSD and the rms values.

Table 3: Simulation parameters [46].

Parameter	value	Parameter	value
m_s	*8016 kg*	k_z	*185 kN/m*
m_3	*42.6 kg*	k_y	*185 kN/m*
m_4	*42.6 kg*	k_t	*125kNm/rad*
m_{ur}	*1500 kg*	c_z	*4000 Nm.s/rad*
I_{xx}	*10495 kgm*^{2}	c_y	*4000 Ns/m*
I_{yy}	*16353 kgm*^{2}	c_t	*3500 Ns/m*
I_3	*3500 kgm*^{2}	K_{Ti}, *i=1,…,4*	*340 kN/m*
I_4	*3500 kgm*^{2}	C_{Ti}, *i=1,…,4*	*1935 Ns/m*
WB	*3.13 m*	K_{TYi}, *i=1,2*	*256.2 kN/m*
WB_1	*1.23 m*	K_{TYi}, *i=3,4*	*316.2 kN/m*
WB_2	*1.9 m*	C_{TYi}, *i=1,…,4*	*1800 Ns/m*
T	*1.81m*	$h+h_1$	*0.8 m*
R	*0.8 m*	l_y	*0.0 m*
l_x	*0.291 m*	L_0	*0.16 m*

The response acceleration spectra obtained along the vertical, pitch and roll axes are compared with those of the measured data in Fig. 9. The comparisons along the fore-aft and lateral axes, however, were not attempted due to simplifying assumption of constant forward speed, negligible articulation forces and lack of consideration of the tire-terrain interactions in the fore-aft direction. It should be noted that the spectra of the measured accelerations are quite smooth in relation with those derived from the model responses, as seen in Fig. 9. This is attributed to the number of averages performed and signal overlap used during processing of the measured data. While the results suggest comparable trends between the model responses and the measured spectra, considerable deviations are also evident. The model responses exhibit significant troughs near 2 *Hz* and at higher frequencies, which are attributed to the wheelbase filtering effect [42-44]. The deviation in the responses are also attributable to various simplifying modeling assumptions, particularly the consideration of negligible contributions due to articulation forces and moments, absence of wheel hop, and linear tire and suspension properties. Despite the observed deviations, the results in general suggest reasonably good validity of the model for predicting vertical, roll and pitch ride responses of the sprung mass. The model may thus be considered applicable for identifying desirable suspension design parameters for enhanced attenuation of the terrain-induced whole-body vibration.

The ride dynamic responses of the model were further evaluated in terms of unweighted and frequency-weighted vertical, roll and pitch rms accelerations. The computed values of the rms accelerations are compared with those derived from the measured data of the suspended vehicle corresponding to the unloaded condition in Table 4. The results presented in Table 4 suggest good correlations between the frequency-weighted acceleration values of the model and the measured data in the pitch and roll axes. Considerable discrepancy, however, is observed in the vertical acceleration values. Higher vertical acceleration response of the model at frequencies above 3 *Hz* (Fig. 9), where the magnitude of W_k-weighting is relatively larger, contributed to higher frequency-weighted rms value. This is evident from relatively smaller difference in the unweighted vertical acceleration values. The results also illustrate considerably higher values of the unweighted roll and pitch accelerations compared to the weighted values. This is mostly attributed to the properties of the W_e-weighting. Considering the promising potentials of the suspension concept, further efforts would be desirable to formulate a more reliable model so as to derive an optimal suspension design for different classes of off-road vehicles.

Table 4: Comparisons of weighted and unweighted rms accelerations of the suspended vehicle model with the corresponding measured values.

Axis	Unweighted rms accelerations			Frequency-weighted rms accelerations		
	Model	Measured	%Deviation	Model	Measured	%Deviation
z	1.28	1.00	28.0	0.98	0.62	58.0
θ	0.77	0.82	-6.1	0.41	0.43	-3.2
ϕ	1.71	2.00	-14.5	0.49	0.44	10.6

6. Sensitivity analysis and optimization of the torsio-elastic suspension design

Ride performance potentials of the proposed toriso-elastic suspension would be dependent on a number of vehicle design and operating parameters. The stiffness properties and geometry of the torsio-elastic suspension would also affect the load carrying capacity of the suspension. The potential performance benefits of the torsio-elastic suspension are thus further explored through a sensitivity analysis of the ride responses to variations in suspension parameters, namely the linkage length L_0, and stiffness (k_y, k_z, k_t) and damping (c_y, c_z, c_t) properties of the torsio-elastic suspension, while assuming constant forward speed of 5 *km/h* and unloaded condition. The results attained are used to formulate an optimization problem in an attempt to seek an optimal design of the proposed torsio-elastic suspension. Each parameter was varied by ±50% about the nominal value, and the responses were obtained in terms of unweighted and frequency-weighted vertical, pitch and roll rms accelerations. The results revealed nearly negligible effect of the linkage length on the acceleration responses. The influences of variations in stiffness and damping parameters alone on the rms values are thus presented in Table 5.

The results show that both the frequency-weighted and unweighted vertical and pitch rms accelerations are strongly affected by the suspension vertical stiffness. An increase in the pitch and vertical mode resonance frequencies caused by higher vertical stiffness as well as coupling between vertical and pitch modes resulted in higher frequency-weighted and unweighted vertical and pitch accelerations. Variations in the vertical stiffness, however, do not influence the W_e-weighted and unweighted roll accelerations, suggesting that vertical and roll modes of the vehicle are mostly decoupled.

Table 5: Influences of variations in torsio-elastic suspension stiffness and damping properties on the weighted and unweighted rms acceleration responses of the model.

Parameters		Unweighted rms acceleration			Weighted rms acceleration		
		z	θ	ϕ	z	θ	ϕ
Nominal value		**1.28**	**0.77**	**1.71**	**0.98**	**0.41**	**0.49**
k_z	-50%	1.21	0.67	1.72	0.95	0.34	0.49
	+50%	1.40	0.88	1.70	1.05	0.48	0.49
k_y	-50%	1.28	0.77	1.69	0.98	0.41	0.48
	+50%	1.28	0.77	1.73	0.98	0.41	0.49
k_t	-50%	1.28	0.77	1.76	0.98	0.41	0.50
	+50%	1.28	0.77	1.65	0.98	0.41	0.46
c_z	-50%	1.36	0.89	1.71	0.99	0.52	0.49
	+50%	1.26	0.72	1.71	0.98	0.37	0.49
c_y	-50%	1.28	0.77	1.73	0.98	0.41	0.50
	+50%	1.28	0.77	1.70	0.98	0.41	0.48
c_t	-50%	1.28	0.77	1.74	0.98	0.41	0.50
	+50%	1.28	0.77	1.68	0.98	0.41	0.48

While the lateral stiffness variations yield only slight effect on the W_e-weighted roll acceleration, a lower value of torsional stiffness yields higher values of unweighted and W_e-weighted roll acceleration magnitudes. This influence is greater for the unweighted roll response and is most likely caused by the properties of the W_e-weighting. The roll response is mostly affected by the torsional stiffness coefficient, while the effect of lateral stiffness is very small.

While light damping of the torsio-elastic members may not yield important influences on the ride vibration responses, both the weighted and unweighted vertical and pitch accelerations tend to increase with lower vertical damping of the torsio-elastic member. A decrease in c_y and c_t results in slightly higher roll rms acceleration values. The results suggest that a suspension design with lower vertical and lateral stiffness, and higher torsional stiffness would yield lower overall weighted and unweighted rms acceleration magnitudes. Higher values of vertical damping coefficients would also be desirable, while the effects of c_y and c_t are relatively small.

6.1 Optimization variables and objective functions

A design optimization is undertaken to seek optimal torsio-elastic suspension parameters using the Pareto technique based on the Genetic Algorithm (GA) [45]. The W_k-weighted and unweighted rms vertical accelerations, (a_{wz}, a_z), W_e-weighted and unweighted rms pitch and roll accelerations, ($a_{w\theta}$, a_θ) and ($a_{w\phi}$, a_ϕ), are selected as the objective functions to be minimized. The results attained from the sensitivity analysis revealed that the rms acceleration responses are mostly influenced by the vertical, lateral and torsional stiffness, and the vertical damping coefficients. Two objective functions are thus formulated to seek minimal weighted and unweighted rms accelerations, respectively, with parameter design vector $X = \{ k_y, k_z, k_t, c_z \}$, such that:

$$F_w(X) = K_1 a_{wz}(X) + K_2 a_{w\theta}(X) + K_3 a_{w\phi}(X)$$
$$F(X) = K_1 a_z(X) + K_2 a_\theta(X) + K_3 a_\phi(X) \quad (20)$$

where $F_w(X)$ and $F(X)$ are the weighted and

unweighted rms acceleration functions, and K_1, K_2 and K_3 are the weighting factors such that $\sum_{i=1}^{3} K_i = 1$. The minimization function $F_w(X)$ also accounts for the human sensitivity to vibration as reflected by the weighting functions. The solutions of the above minimization functions for vehicle suspensions generally converge towards lower stiffness values, which may tend to result in reduced load carrying capacity and roll stability limits, and greater relative deflections of the sprung mass with respect to the unsprung masses. Although the kinematic effect of the proposed suspension is expected to inhibit the relative deflection, limit constraints are introduced in order to seek solutions within practical ranges, such that: $30 \leq k_y \leq 300$ *kN/m;* $70 \leq k_z \leq 300$ *kN/m;* $50 \leq k_t \leq 250$ *kNm/rad;* and $3 \leq c_z \leq 9$ *kN.s/m.*

The solutions of the minimization problems were obtained in terms of sets of Pareto optimal solutions. As an example, Fig. 10 illustrates the various Pareto optimal solutions in terms of the weighted acceleration values. The optimal solutions in weighted vertical, roll and pitch accelerations suggest a positive correlation between $a_{w\theta}$ and a_{wz} attributed to greater coupling between the vertical and pitch modes. Fig. 10(a), however, suggests a weaker coupling between roll and vertical accelerations, while the coupling between roll and pitch responses is negligible, as seen in Fig. 10(c). Similar trends in optimal Pareto solutions were also observed for the unweighted rms accelerations. These solutions were subsequently explored to identify a design compromise that would yield minimal values of the multi-objective functions, defined in Eq. (20), using different combinations of the weighing factors. The results revealed nearly negligible effect of the roll acceleration weighting (K_3), as expected due to its relatively lower coupling with the vertical and pitch responses. The optimal solution and the corresponding design parameters were thus identified by placing greater weighting for a_{wz} (K_1=*0.5* to *0.7*) and $a_{w\theta}$ (K_2=*0.2* to *0.4*). The combination (K_1=*0.6,* K_2=*0.3,* K_3=*0.1*) resulted in minimal values of the vertical, pitch and roll acceleration responses, which resulted in the follows optimal design vectors:

$X = \{ k_y, k_z, k_t, c_z \} = \{ 91.8, 71.3, 204.8, 8.3 \}$; for the weighted function.

$X = \{ k_y, k_z, k_t, c_z \} = \{ 36.4, 73.3, 187.5, 6.3 \}$; for the unweighted function.

The above results show comparable values of the suspension parameters for both the minimization functions, except for the values of k_y. The minimization of weighted function converged towards a considerable greater value of k_y compared to that for the unweighted function. The minimization of the weighted values in roll tends to converge towards a higher value of k_y in order to achieve roll mode frequency well above the dominant frequency range of the W_e-filter (1-2 *Hz*). The resulting optimal solutions in terms of both the weighted and unweighted rms accelerations and the design parameters are summarized in Table 6.

Table 6: Optimal values of the acceleration responses.

Axis	Unweighted rms acceleration (m/s^2)			Weighted rms acceleration (m/s^2)		
	Nominal	optimal	% change	Nominal	optimal	% change
z	1.28	1.21	-5.46	0.98	0.93	-5.10
θ	0.77	0.62	-19.48	0.41	0.32	-21.95
ϕ	1.71	1.65	-3.51	0.49	0.46	-6.12

The results in Table 6 show that the optimal suspension design yields considerably lower values of $a_{w\theta}$ and a_θ compared to those of the model with nominal parameters, while the reductions in vertical (a_{wz}, a_z) and roll ($a_{w\phi}$, a_ϕ) acceleration values are relatively small, ranging

from roughly 3.5 to 6%. The relative deflection responses of the sprung mass with respect to the rear axle were further evaluated to study the effects of optimal parameters on the vertical and roll deflections. The results revealed relatively higher relative deflections of the optimal suspension compared to the nominal suspension parameters, although the increases were considered could be small. The rms vertical relative deflection of the model with optimal suspension was 4.8 *cm* compared to 4.0 *cm* for the nominal suspension model.

7. Conclusions

The ride performance potentials of a novel torsio-elastic suspension were investigated for a forestry vehicle through field assessments and simulations of a ride dynamic model. The results attained from the field measurements revealed significant benefits of the rear axle torsio-elastic suspension in reducing the operator vibration exposure. In the loaded case, the suspended vehicle resulted in 35%, 43% and 57% reductions in the frequency-weighted rms accelerations along the *x*-, *y*- and *z*-axis, respectively, compared to the unsuspended vehicle. The suspended vehicle, however, revealed slightly higher unweighted pitch and roll rms accelerations, when unloaded, while the unweighted rms accelerations along the *x*-, *y*- and *z*-axis were 44%, 27% and 45% lower, respectively, compared to those of the unsuspended vehicle. The results further showed that the magnitudes of horizontal vibration transmitted to the operator's station were either comparable to or exceeded the vertical vibration magnitude. While the ride model responses agreed reasonably well with the measured responses in vertical, roll and pitch axes, the model could not be applied to predict fore-aft and lateral ride responses due to various simplifying assumptions, namely constant forward speed, negligible contributions due to articulation forces and moments, and lack of tire-terrain interaction in the shear axes.

The results obtained from sensitivity suggested that a suspension design with lower vertical and lateral stiffness but higher torsional stiffness would yield lower overall unweighted and weighted rms acceleration magnitudes. The results also suggested strong coupling between vertical and pitch mode responses, but negligible coupling between the pitch and roll modes of the vehicle. The optimal suspension parameters identified from solutions of a multi-objective minimization problem resulted in further considerable reductions in the pitch rms accelerations in the order of 20%, with only 3.5 to 6% reductions in vertical and roll accelerations. Considering the notable performance benefits of the proposed suspension, it would be desirable to develop more reliable ride and handling dynamic models of the vehicle, which could serve as a vital tool for suspension design and assessments of the ride vibration and handling/roll dynamics of a broader class of off-road vehicles.

References

1. Boileau PE and Rakheja S (1990) Vibration attenuation performance of suspension seats for off-road forestry vehicles. Int J of Industrial Ergonomics, 5, 275-291.
2. ISO-2631-1 (1997) Evaluation of human exposure to whole-body vibration. Part 1: General requirements. International Organization for Standardization, Geneva.
3. Cation S, Jack RJ, Dickey JP, Lee-Shee N and Oliver M (2008) Six degree of freedom whole-body vibration during forestry skidder operations. Int J of Industrial Ergonomics, 38, 739-757.
4. Neitzel R and Yost, M (2002) Task-based assessment of occupational vibration and noise exposure in forestry workers. AIHA Journal, 63, 617-627.

5. Commission of the European Communities (1992) Proposal for a council directive on the minimum health and safety requirements regarding the exposure of workers to the risks arising from physical agent. Brussels, Belgium.
6. Sherwin LM, Owende PMO, Kanali CL, Lyons J. and Ward SM (2004) Influence of forest machine function on operator exposure to whole-body vibration in a cut-to-length timber harveste. Ergonomics, 47, 1145–1159.
7. Seidel H (2005) On the relationship between whole body vibration exposure and spinal health risk. Industrial Health, 43, 361-377.
8. Calvo A (2009) Musculoskeletal disorders (MSD) risks in forestry: a case study to propose an analysis method. Agricultural Engineering International: The CIGR EJournal, 6.
9. Korhonen O, Nummi J, Nurminen M, Nygard K, Soininen H and Wiikeri M (1980) Finnish lumberjacks. Part 3: the health of forest tractor drivers. Institute of Occupational Health, Helsinki.
10. Bovenzi M, Zadini A, Franzinelli A and Borgogni F (1991) Occupational musculoskeletal disorders in the neck and upper limbs of forestry workers exposed to hand-arm vibration. Ergonomics, 34, 547-562.
11. Bovenzi M, Pinto L and Stacchini N (2002) Low back pain in port machinery operators, Journal of Sound and vibration. 253, 3-20.
12. Bovenzi M, Hulshof CTJ (1998) An updated review of epidemiologic studies on the relationship between exposure to whole-body vibration and low back pain. Journal of Sound and Vibration, 215, 595-611.
13. Bovenzi M, Rui F, Negro C, D'Agostin F, Angotzi G, Bianchi S, Bramanti L, Festa G, Gatti S, Pinto L, Rondina L and Stacchini N(2006) An epidemiological study of low back pain in professional drivers. Journal of Sound and Vibration, 298, 514–539.
14. Hansson P-A (2002) Working space requirement for an agricultural tractor axle suspension. Biosystems Engineering, 81, 57-71.
15. Claar PW, Sheth P, N, Buchele WF and Marley SJ (1980) Agricultural tractor chassis suspension system for improved ride comfort. ASAE Paper 80-1565.
16. Crolla DA and MacLaurin EB, (1985) Theoretical and practical aspects of the ride dynamics of off-road vehicles—Part 1. J of Terramechanics, 22, 17–25.
17. Hansson, P-A. (1996) Rear axle suspension with controlled damping on agricultural tractors. Computers and Electronics in Agriculture 15, 123–147.
18. Boileau PE, Emile P and Rakheja S (1990) Vibration attenuation performance of suspension seats for off-road forestry vehicles. Int J of Industrial Ergonomics, 5, 275-291.
19. Springfeldt B (1996) Rollover of tractors- International experiences. Safety Science, 24, 95-110.
20. Franklin R, Mitchell R, Driscoll T and Fragar L (2000) Farm related fatalities in Australian, 1989–1992. Australian Centre for Agricultural Health and Safety and Rural Industries Research and Development Corporation, Moree, Australia.
21. Wu X, Rakheja S and Boileau, PE (1999) Dynamic Performance of Suspension Seats Under Vehicular Vibration and Shock Excitations. Transactions of SAE, Passenger Car Journal, 108, 2398-2410.
22. Boileau P.-É., Wu X. and Rakheja S (1998) Definition of a set of idealized values to characterize seated body biodynamic response under vertical vibration. Journal of Sound and Vibration, 215, 841-862.

23. Wu X, Griffin MJ (1998) The Influence of end-stop buffer characteristics on the severity of suspension seat end-stop impacts. Journal of Sound and Vibration, 215, 989–996.
24. Wegscheid E (1994) Another look at skidder ride vibration. J of Forest Engineering, 5, 21-32.
25. Hansson P-A (1995) Optimization of agricultural tractor cab suspension using the evolution method. Computers and Electronics in Agriculture, 12, 35–49.
26. Rakheja S and Sankar S (1984) Suspension design to improve tractor ride: II passive cab suspension. SAE Transactions, 4, 1105–1112.
27. Boulanger P, Lemerle P and Poirot R (2002) A simplified method to design a suspension cab for counterbalance trucks. J of Sound and Vibration, 253, 283–293.
28. Marcu FM, Ahmadian M, Southward S and Jansson S (2009) A methodology for laboratory testing of truck cab suspension. SAE paper 2009-01-2862.
29. Ahmadian M, Patricio P (2004) Effect of panhard rod cab suspension on heavy truck ride measurements. SAE paper 2004-01-2710.
30. Matthews J (1965) Ride comfort for tractor operators III. Investigation of tractor dynamics by analog computer simulation. J of Agricultural Engineering Research, 10.
31. Crolla DA (1980) A theoretical analysis of the ride vibration of agricultural tractors and trailer combinations. Vehicle System Dynamics, 9, 236-260.
32. Wu Qi-Ya, Qing-Za S, Jin-Wen W and Yong-Fa F (1988) The simplified dynamic model, measurement and evaluation of ride vibration for the combination unit of agricultural hand tractor and trailer. Vehicle System Dynamics, 13, 367-385.
33. Cole DJ, and Cebon D (1998) Front-rear interaction of a pitch-plane truck model. Vehicle System Dynamics, 30, 117-141.
34. Logdanoff JL, Kozin F, and Cote LJ (1996) Atlas of off-road ground roughness PSDs and report on data acquisition techniques. ATAC Components Research and Development Laboratories Technical Report No.9387 (LL109), U.S. Army Tank-Automotive Center, Warren, Mich.
35. Robson JD (1979) Road surface description and vehicle response. Int J of Vehicle Design, 1(1), 25-35.
36. Maclaurin B (1983) Progress in british tracked vehicle suspension system. SAE technical series paper No. 830442, International Congress and Exposition, Detroit, Mich.
37. Laib L (1995) Analysis of the vibration-excitation effect caused by deformable soil surface. J of Terramechanics, 32, 151-163.
38. Park S, Popov AA, and Cole DJ (2004) Influence of soil deformation on off-road heavy vehicle suspension vibration. J of Terramechanics, 41, 41-68.
39. Wong JY (2002) Theory of ground vehicles. John Wiley & Sons, New York, 3rd Edition.
40. Matlab Optimization Toolbox User's Guide (1990 – 2001) by The MathWorks, Inc.
41. FERIC/FP Innovations (1979) The forestry engineering research institute of Canada. Montreal, Canada.
42. Cao D, Rakheja S, and Su C-Y (2008) Heavy vehicle pitch dynamics and suspension tuning. Part I: unconnected suspension. Vehicle System Dynamics, 46, 931-953.
43. Sharp RS (2002) Wheelbase filtering and automobile suspension tuning for minimization motion in pitch. Journal of Automobile Engineering, 216, 933-946.
44. Best A (1984) Vehicle ride-stages in comprehension. Phys. Technol., 15, 205-210.
45. Haupt RL, Haupt SE (2004) Genetic Alghorithms. John Wiley & Sons, New York, 2nd Edition.

46. Boileau PE, Emile P and Rakheja S (1996) Évaluation et étude du comportement dynamique d'un système de suspension torsio-élastique pour véhicules tout terrain, Études et recherches, Rapport R-124, Montréal, IRSST.

Appendix: Tire and suspension forces and moments

The vertical (F_{Ti}) and lateral (F_{TYi}) tire forces developed at the tire-road interface (F_{Ti} and F_{TYi}) are derived from the following, where $i = 1, 2$ denote the front axle tires, and $i = 3, 4$ refer to the rear axle tires.

$$\begin{aligned} F_{Ti} &= K_{Ti}[z_s + (-1)^{i+1} T\phi_s - WB_1\theta_s - z_{0i}] + C_{Ti}[\dot{z}_s + (-1)^{i+1} T\dot{\phi}_s - WB_1\dot{\theta}_s - \dot{z}_{0i}] \qquad i = 1, 2 \\ F_{Ti} &= K_{Ti}[z_{ur} + (-1)^{i+1} T\phi_{ur} - z_{0i}] + C_{Ti}[\dot{z}_{ur} + (-1)^{i+1} T\dot{\phi}_{ur} - \dot{z}_{0i}] \qquad i = 3, 4 \end{aligned} \tag{I-1}$$

$$\begin{aligned} F_{TYi} &= K_{TYi}[y_s - (h + h_1 + R)\phi_s] + C_{TYi}[\dot{y}_s - (h + h_1 + R)\dot{\phi}_s] \qquad i = 1, 2 \\ F_{TYi} &= K_{TYi}[y_{ur} - R\phi_{ur}] + C_{TYi}[\dot{y}_{ur} - R\dot{\phi}_{ur}] \qquad i = 3, 4 \end{aligned} \tag{I-2}$$

where K_{Ti} and K_{TYi} are the linear vertical and lateral stiffness and C_{Ti} and C_{TYi} are the linear vertical and lateral damping coefficients of tire *i*, respectively.

The vertical forces developed by the torsio elastic suspension acting on the sprung mass (F_{z3} and F_{z4}) and on the unsprung mass (F_{z3u} and F_{z4u}) are given by:

$$\begin{aligned} F_{z3} &= k_z[z_s - \left(z_3 - \frac{L_0}{2}\phi_3\right) + L_1\phi_s + WB_2\theta_s] + c_z[\dot{z}_s - \left(\dot{z}_3 - \frac{L_0}{2}\dot{\phi}_3\right) + L_1\dot{\phi}_s + WB_2\dot{\theta}_s] \\ F_{z4} &= k_z[z_s - \left(z_4 + \frac{L_0}{2}\phi_4\right) - L_1\phi_s + WB_2\theta_s] + c_z[\dot{z}_s - \left(\dot{z}_4 + \frac{L_0}{2}\dot{\phi}_4\right) - L_1\dot{\phi}_s + WB_2\dot{\theta}_s] \end{aligned} \tag{I-3}$$

$$\begin{aligned} F_{z3u} &= k_z[z_3 + \frac{L_0}{2}\phi_3 - z_{ur} - (L_1 + L_0)\phi_{ur}] + c_z[\dot{z}_3 + \frac{L_0}{2}\dot{\phi}_3 - \dot{z}_{ur} - (L_1 + L_0)\dot{\phi}_{ur}] \\ F_{z4u} &= k_z[z_4 - \frac{L_0}{2}\phi_4 - z_{ur} + (L_1 + L_0)\phi_{ur}] + c_z[\dot{z}_4 - \frac{L_0}{2}\dot{\phi}_4 - \dot{z}_{ur} + (L_1 + L_0)\dot{\phi}_{ur}] \end{aligned} \tag{I-4}$$

where k_z and c_z are the vertical stiffness and damping coefficients of the torsio-elastic suspension. The lateral forces developed by the torsio-elastic suspension acting on the sprung mass (F_{y3} and F_{y4}) and the unsprung mass (F_{y3u} and F_{y4u}) are given by:

$$\begin{aligned} F_{y3} &= k_y[y_s - h\phi_s - y_3] + c_y[\dot{y}_s - h\dot{\phi}_s - \dot{y}_3] \\ F_{y4} &= k_y[y_s - h\phi_s - y_4] + c_y[\dot{y}_s - h\dot{\phi}_s - \dot{y}_4] \end{aligned} \tag{I-5}$$

$$\begin{aligned} F_{y3u} &= k_y[y_3 - h_1\phi_{ur} - y_{ur}] + c_y[\dot{y}_3 - h_1\dot{\phi}_{ur} - \dot{y}_{ur}] \\ F_{y4u} &= k_y[y_4 - h_1\phi_{ur} - y_{ur}] + c_y[\dot{y}_4 - h_1\dot{\phi}_{ur} - \dot{y}_{ur}] \end{aligned} \tag{I-6}$$

where k_y and c_y are the lateral stiffness and damping coefficients of the torsio-elastic suspension. The roll moments developed by the torsio-elastic suspension acting on the sprung mass ($M_{\theta 3s}$ and $M_{\theta 4s}$) and the unsprung mass ($M_{\theta 3u}$ and $M_{\theta 4u}$) are defined from:

$$M_{\theta 3s} = k_t(\phi_s - \phi_3) + c_t(\dot{\phi}_s - \dot{\phi}_3)$$
$$M_{\theta 4s} = k_t(\phi_s - \phi_4) + c_t(\dot{\phi}_s - \dot{\phi}_4) \quad \text{(I-7)}$$

$$M_{\theta 3u} = k_t(\phi_3 - \phi_{ur}) + c_t(\dot{\phi}_3 - \dot{\phi}_{ur})$$
$$M_{\theta 4u} = k_t(\phi_4 - \phi_{ur}) + c_t(\dot{\phi}_4 - \dot{\phi}_{ur}) \quad \text{(I-8)}$$

where k_t and c_t are the torsional stiffness and damping coefficients of the torsio-elastic suspension, respectively.

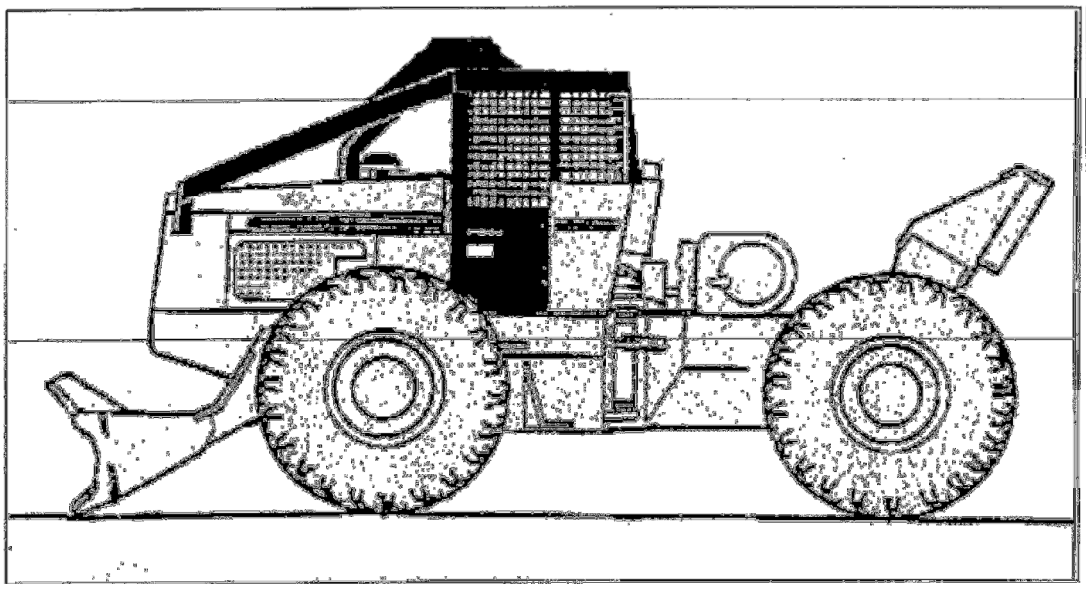

Figure 1: Schematic of a wheeled forestry skidder.

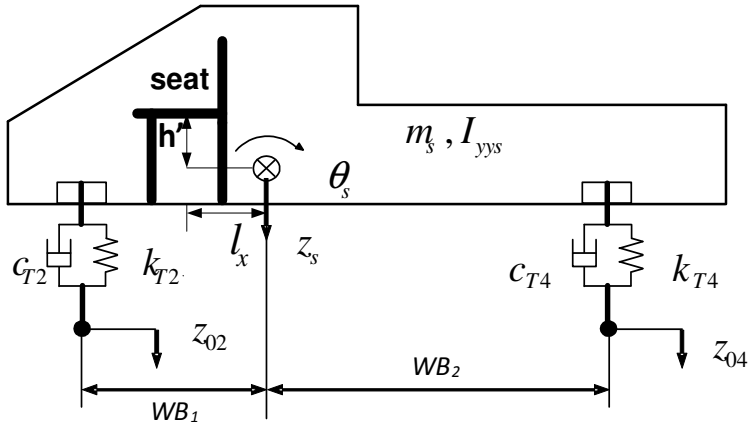

(a)

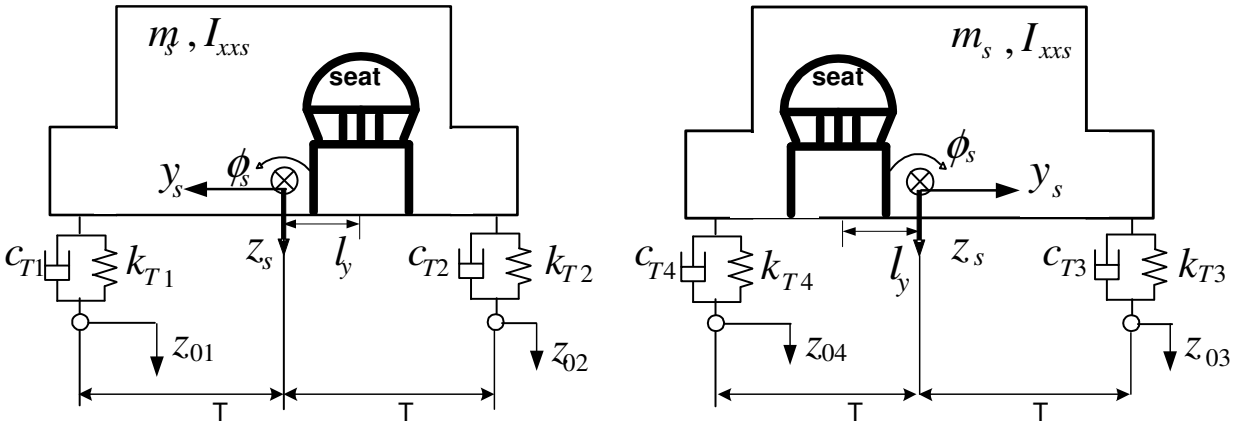

(b) (c)

Figure 2: Pitch- and roll-plane representations of a conventional skidder: (a) pitch-plane; (b) roll-plane, (front axle; front view); and (c) roll-plane, (rear axle; rear view).

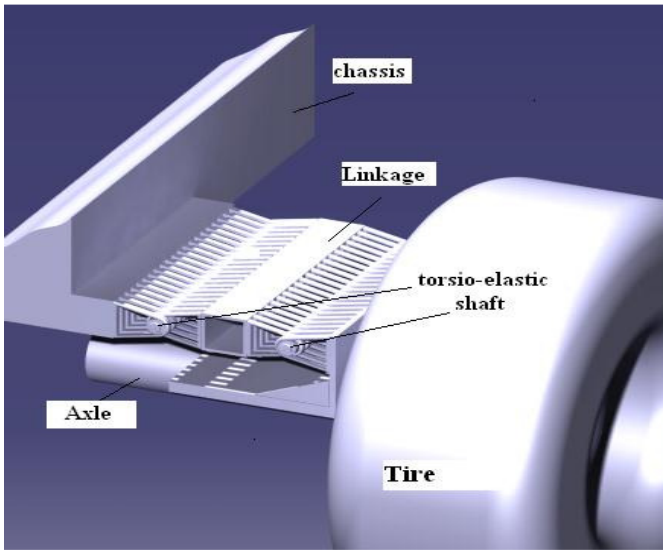

(a)

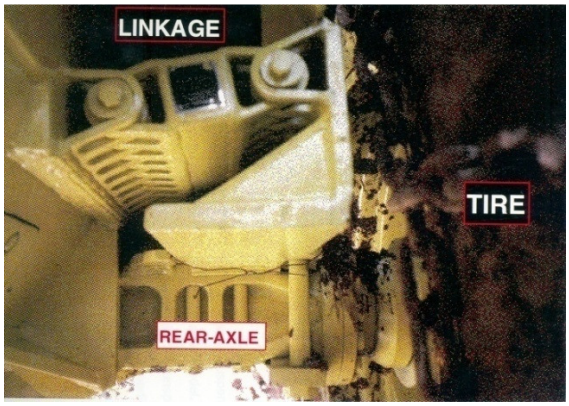

(b)

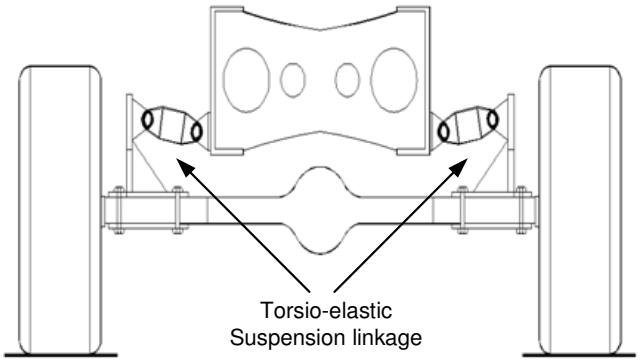

(c)

Figure 3: The prototype rear-axle torsio-elastic suspension: (a) isometric schematic; (b) pictorial view; and (c) roll-plane illustration of the suspension.

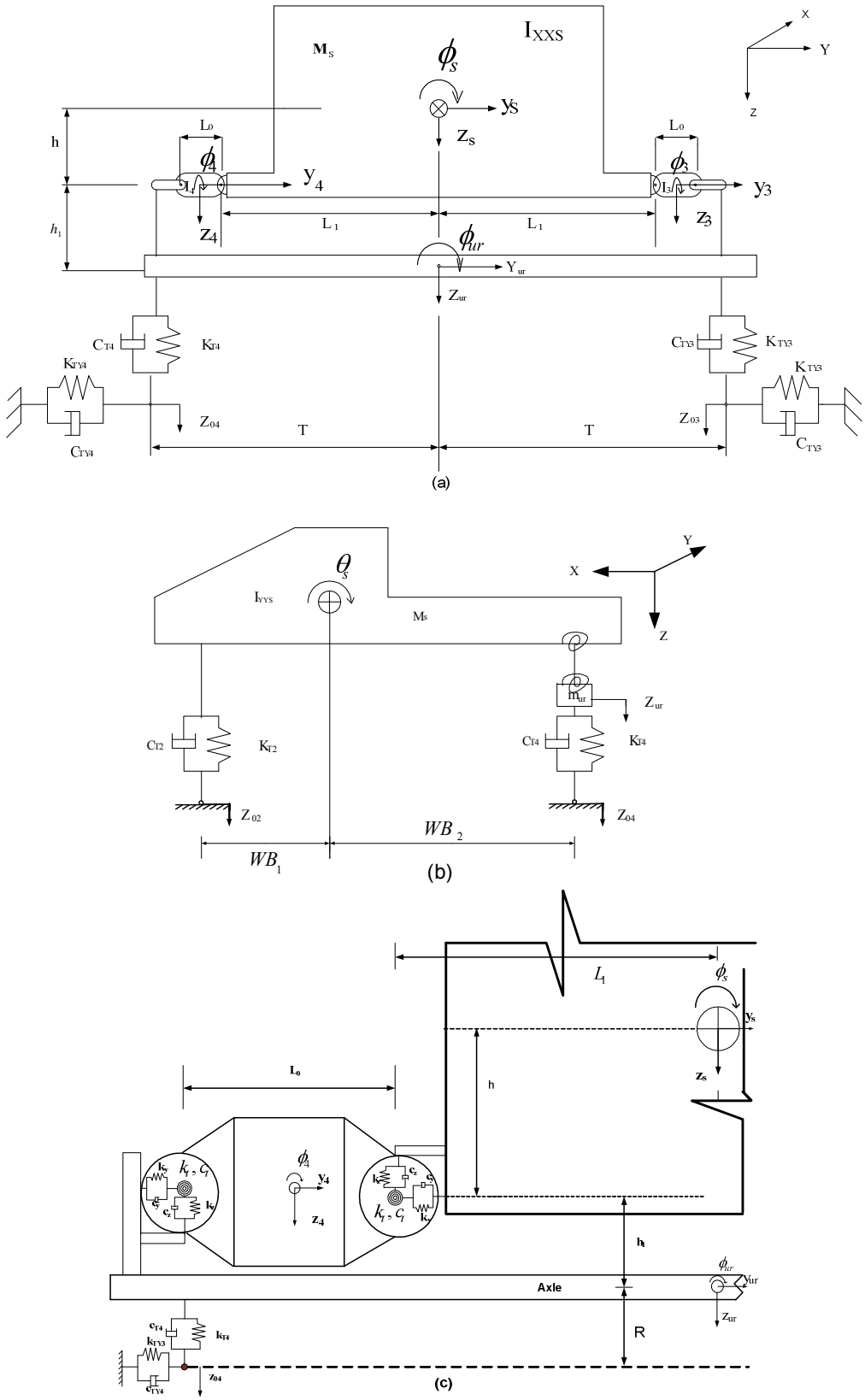

Figure 4: Schematic representation of the 13-DOF suspended vehicle model: (a) roll-plane; (b) pitch-plane; and (c) torsio-elastic suspension linkage mechanism.

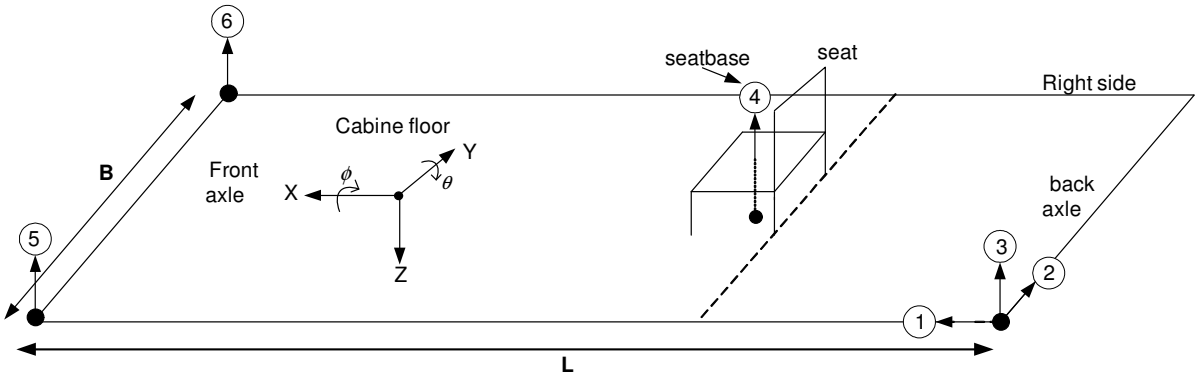

Figure 5: Locations of accelerometers on the cabin floor: "1", "2"and "3", oriented along the x , y and z -axes at the rear-left, respectively; "4" at the seat base along z -axes; "5" front-left along z -axes; and "6" front-right along z -axes.

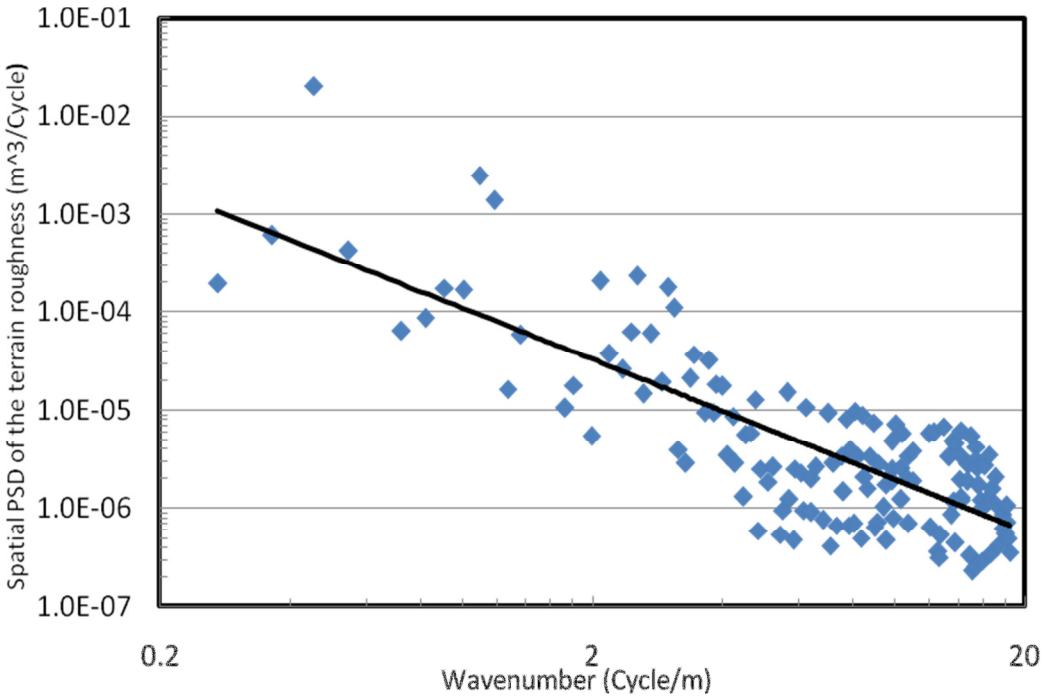

Figure 6: Spatial spectral density of terrain elevation identified from measured data at various discrete frequencies and the power regression curve $\left(r^2 = 0.6425\right)$.

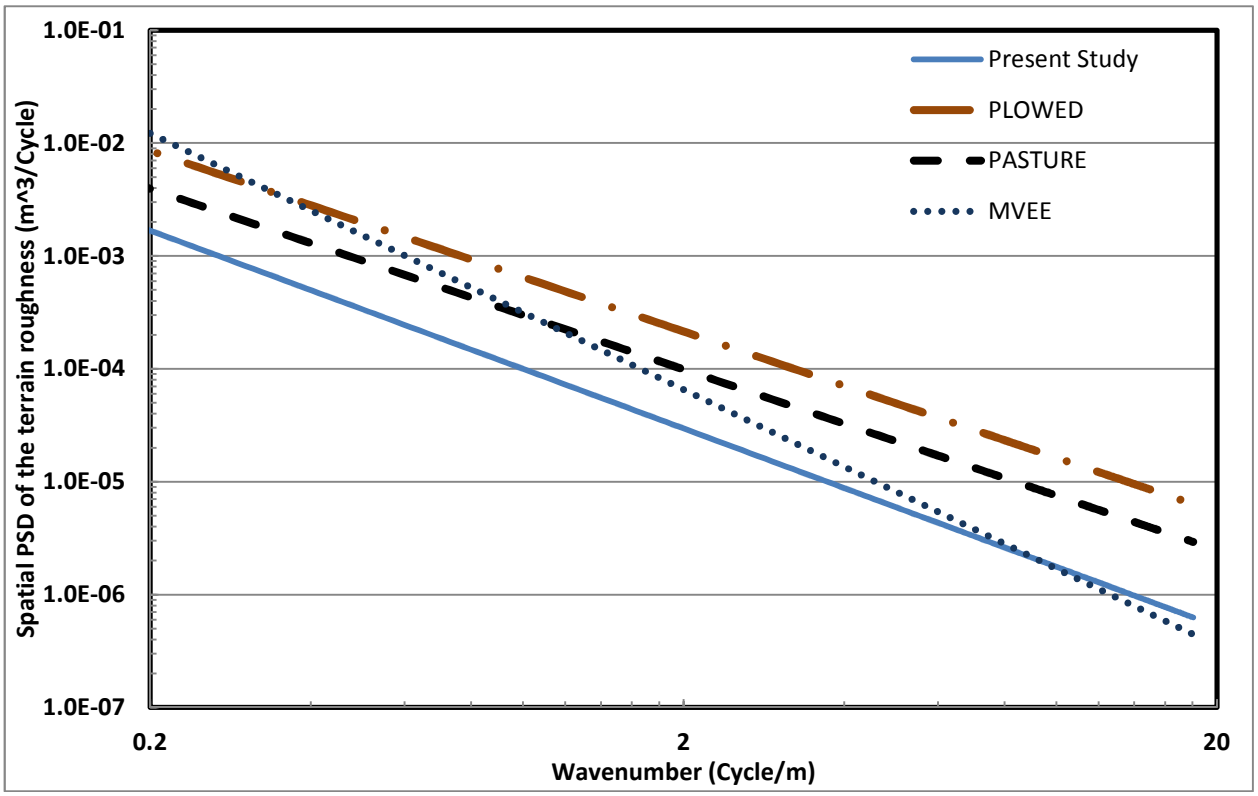

Figure 7: Comparisons of roughness profiles of some of the off-road terrains with that estimated for the forestry terrain.

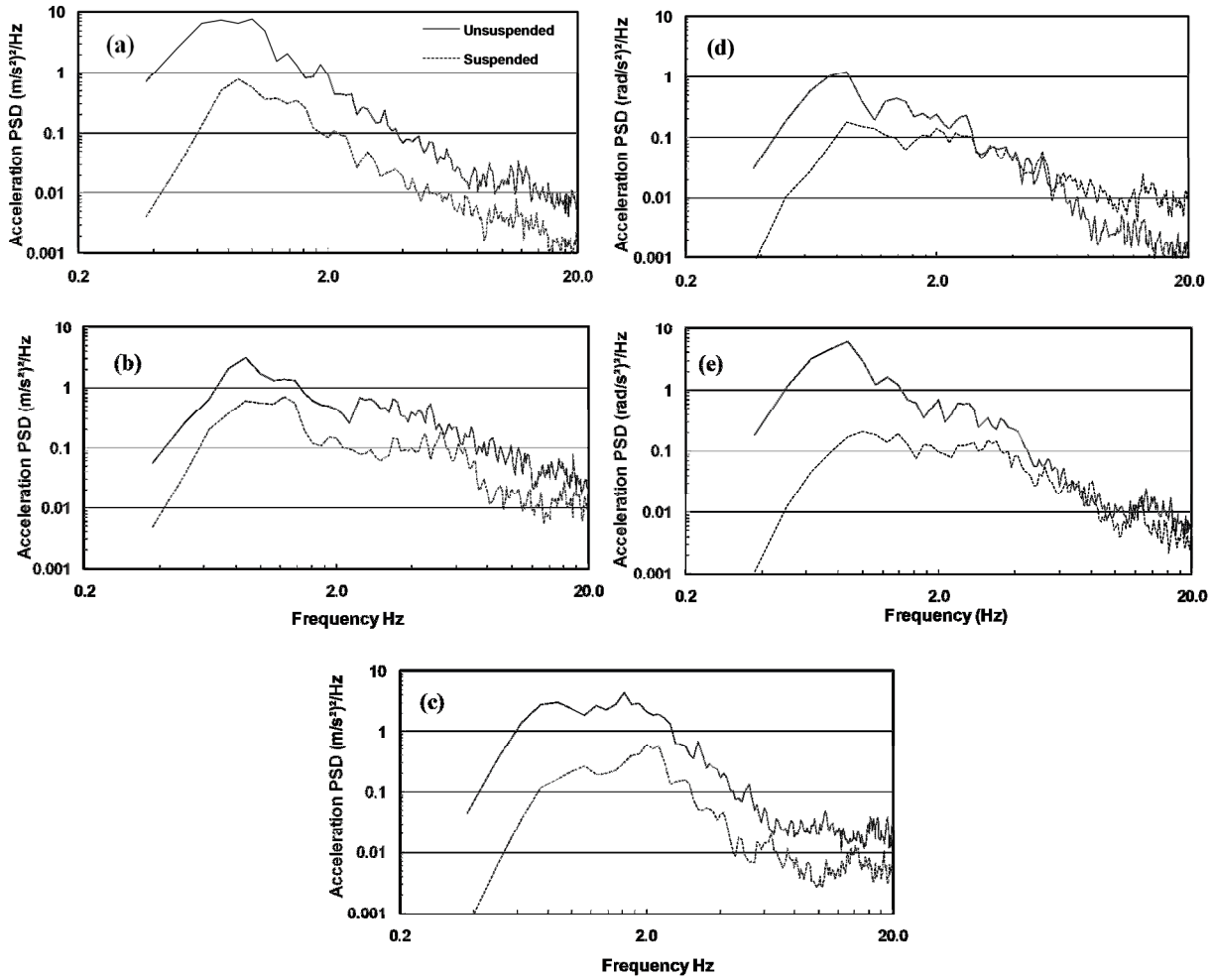

Figure 8: Comparisons of measured acceleration PSD responses at the cab floor of the suspended and unsuspended vehicles: (a) fore-aft; (b) lateral; (c) vertical; (d) pitch; and (e) roll.

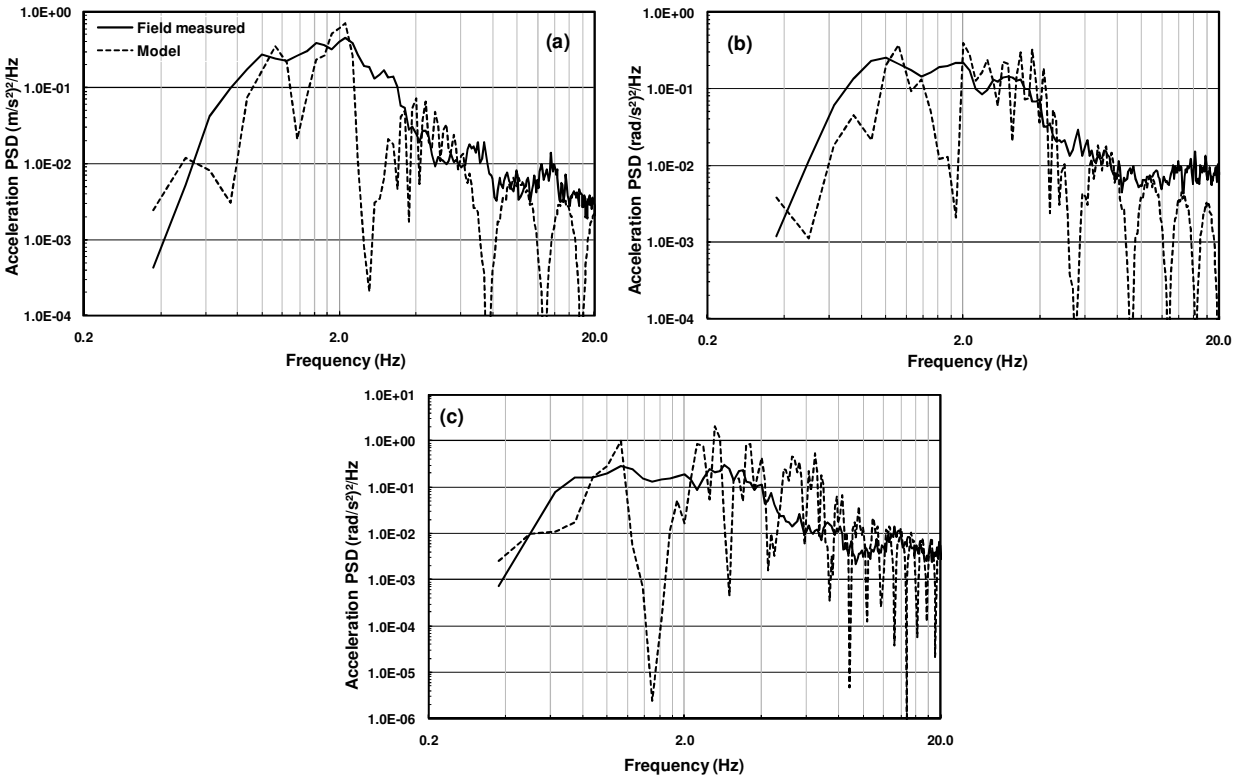

Figure 9: Comparisons of acceleration PSD responses of the suspended vehicle model with those of the measured data: (a) vertical; (b) pitch; and (c) roll.

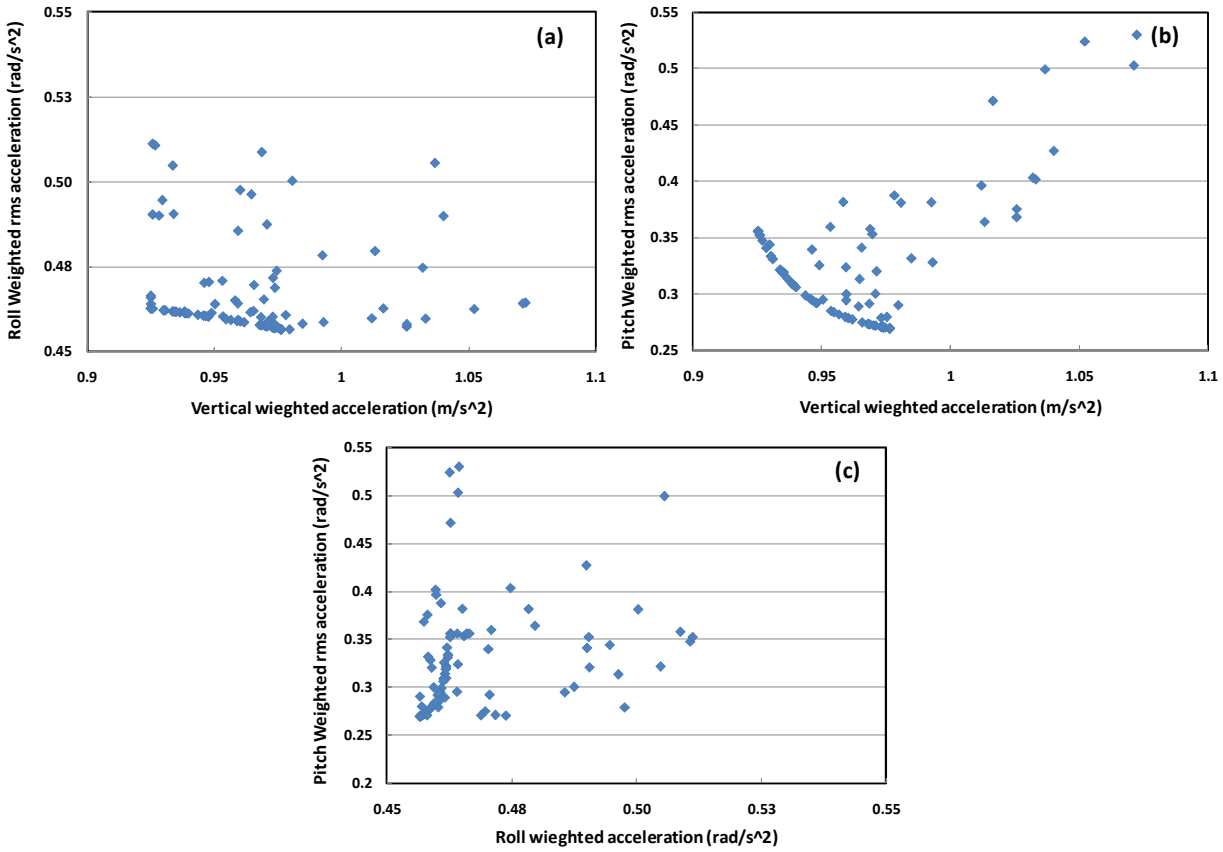

Figure 10: Pareto optimal solutions for weighted accelerations responses: (a) roll *vs* vertical acceleration; (b) pitch *vs* vertical acceleration; (c) pitch *vs* roll acceleration.